Measuring the Tensorial Flow of Mosaic Vector Beams in Disordered Media

Davide Pierangeli,[1,*] Andrea Aiello,[2] and Claudio Conti[3]
[1]Institute for Complex Systems, National Research Council, Via dei Taurini 19, 00185 Rome, Italy
[2]Max Planck Institute for the Science of Light, Staudtstrasse 2, 91058 Erlangen, Germany
[3]Department of Physics, Sapienza University of Rome, P.le Aldo Moro 5, 00185 Rome, Italy

(Received 24 December 2023; revised 14 March 2024; accepted 15 May 2024; published 11 June 2024)

Optical beams with nonuniform polarization offer enhanced capabilities for information transmission, boasting increased capacity, security, and resilience. These beams possess vectorial features that are spatially organized within localized three-dimensional regions, forming tensors that can be harnessed across a spectrum of applications spanning quantum physics, imaging, and machine learning. However, when subjected to the effect of the transmission channel, the tensorial propagation leads to a loss of data integrity due to the entanglement of spatial and polarization degrees of freedom. The challenge of quantifying this spatial-polarization coupling poses a significant obstacle to the utilization of vector beams in turbulent environments, multimode fibers, and disordered media. Here, we introduce and experimentally investigate *mosaic* vector beams, which consist of localized polarization *tesserae* that propagate in parallel, demonstrating accurate measurement of their behavior as they traverse strongly disordered channels and decoding their polarization structure in single-shot experiments. The resultant transmission tensor empowers polarization-based optical communication and imaging in complex media. These findings also hold promise for photonic machine learning, where the engineering of tensorial flow can enable optical computing with high throughput.

DOI: 10.1103/PhysRevLett.132.243801

Vector beams are electromagnetic fields characterized by a polarization profile that varies in space [1,2]. Numerous studies have showcased their profound impact on photonics applications [3], catalyzing advancements in metrology [4–10], quantum information processing [11–13], spintronics [14], and optical communication [15–19]. Notably, vectorial structured light has facilitated the characterization of quantum channels using classical light [20], high-dimensional quantum cryptography [21], all-optical neural networks [22], and the development of diffractive transformers [23].

Despite their significant potential, the utilization of vector beams in complex media remains a formidable challenge. These beams are highly susceptible to strong mode-mixing, turbulence, and disorder, factors that disrupt their vectorial structure [24–28]. Retrieving the original polarization information becomes a daunting task, given the absence of a readily measurable quantity that encodes the vectorial scattering process.

In this Letter, we present the first experimental measurement of the *tensorial flow* characterizing the propagation of *mosaic* vector beams through a disordered channel. Mosaic beams encode a varying polarization within spatially localized regions, offering a framework for designing a method to measure multidimensional information and the resulting transmission tensor in complex media. These beams are constructed from *tesserae* whose scattering can be rigorously analyzed. We introduce and validate a simple noninterferometric technique for measuring the effective part of the transmission tensor using a minimal set of intensity images. This real-valued tensor is a quantity practically useful in experiments. By harnessing the measured four-index tensor, we successfully decode polarization information through a strongly scattering medium. From a single-shot intensity detection of the speckle pattern, we accurately retrieve four polarization modes. These results pave the way for novel approaches to communication and imaging using polarization-structured light. Given the pivotal role of tensors in machine learning, we anticipate that our measurement will also provide a valuable tool for optical computing by enabling the engineering of tensorial propagation.

The transmission of vector beams through complex media has been the subject of intense debate. Recent findings have proven the polarization pattern is nonresistant to aberrations and turbulence [27]. Only a global property of the beam—the vectorness—has been found invariant under perturbations within the optical path, which suggests that alternative bases are necessary for robust multimode communication [28]. Moreover, any robustness to perturbations is lost in the case of strongly disordered media that affect both the polarization and spatial degree of freedom, i.e., for the so-called two-sided channels. Retrieving the input polarization structure through these channels is the critical problem that we solve in this Letter. Recently, we have proved polarization reconstruction by passing the

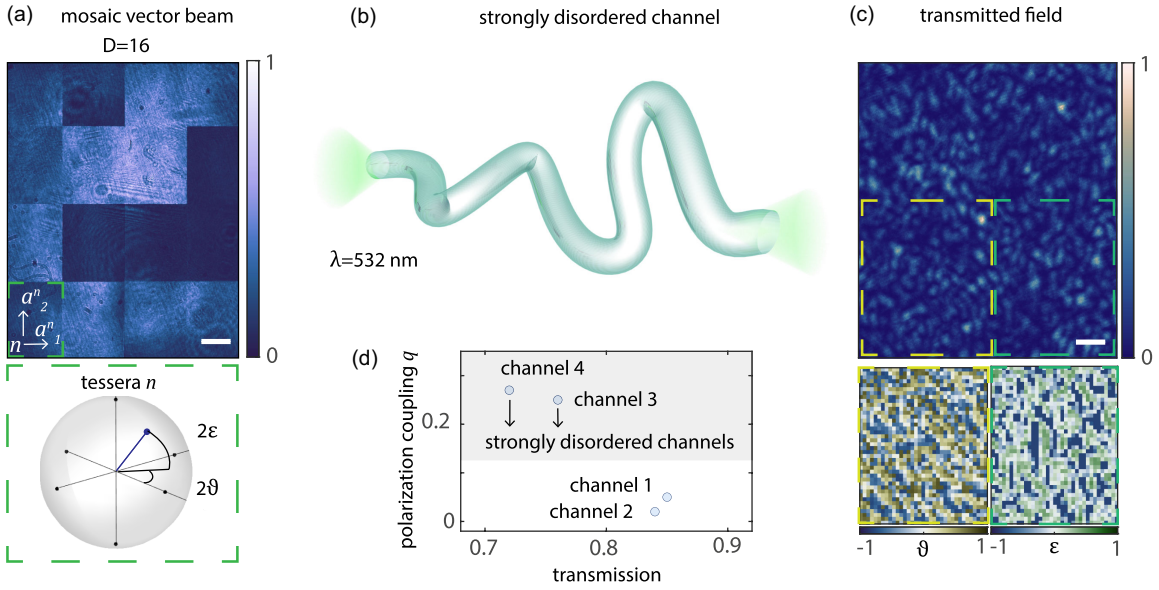

FIG. 1. Scattering of vector beams in disordered channels. (a) A mosaic vector beam composed of $D = 16$ tesserae of uniform polarization. The image shows the right-circular intensity of a generated beam with randomly selected SOPs. The field in the nth tessera is illustrated on the Poincaré sphere. Scale bar is 1 mm. (b) Sketch of a strongly disordered channel, for example, a twisted and bent multimode fiber or an opaque medium. (c) The transmitted intensity is a speckle pattern with no trace of the input mosaic. The inset false-color maps are the spatially resolved azimuth and ellipticity angle over output modes of size of 10×10 pixels. (d) Polarization coupling parameter q measured for four different glass diffusers. Scatterers lying in the gray area, which couple the field in space and polarization, are referred to as strongly disordered channels.

vector beam in a scattering medium and using supervised learning [29]. In that approach, the transmission channel representing the scatterer is regarded as a black box whose properties remain unknown. Conversely, here we first use designed mosaics to determine the transmission tensor of the medium, furnishing a description of the unknown channel. Then, we exploit the knowledge of the tensor to reconstruct any mosaic beam without machine learning techniques. The result is twofold: we give a solid foundation to machine learning polarimetry [29] and we provide a new method for characterizing the transmission of disordered media and unscrambling vectorial structured light.

Figure 1 reports an illustration of our system. Details on the experimental setup are reported in Supplemental Material [30]. The input mosaic beam is made by D uniform states of polarization (SOPs) in separated spatial blocks (tesserae). These wave functions provide spatially orthogonal optical states and allow studying the propagation of nonuniformly polarized light in terms of discrete input-output modes. They can be generated easily by phase-only spatial light modulators (SLMs). In Fig. 1(a) we show the measured intensity of a mosaic beam generated at $\lambda = 532$ nm, composed by $D = 16$ tesserae with random SOP. The continuous-wave laser beams are made to propagate through a thick glass diffuser that acts as a strongly disordered channel [Fig. 1(b)]. The far-field transmission shows a speckle intensity with no trace of the input spatial partitions. The output polarization varies from point to point in a disordered way. As shown in Fig. 1(c), the azimuth angle θ and ellipticity ε of the SOP [34] have random values in each output mode. This indicates the mixing of the input SOPs and the coupling between polarization and spatial degrees of freedom. To quantify the amount of space-polarization coupling induced by the scatterer, we send L uniform beams ($D = 1$) having the ith Stokes parameter $S_i = 0$, we measure the corresponding output $|S_i|$ averaged over space [35], and evaluate the polarization coupling parameter as $q = \sum^L |S_i|/L$. We test four diffusers with different grits. Figure 1(d) reports q versus the total transmission for the four samples (channels 1–4). We observe that channels exhibit either near-zero or large q values, two distinct conditions referred to as weak and strong coupling. In weak coupling, the channel maintains the input SOP and affects only the spatial degree of freedom (one-sided channel). The measured degree of polarization is high ($\nu \simeq 0.97$). The speckle pattern is developed without polarization scrambling [36]. On the contrary, in strong coupling, the output light appears depolarized [see Fig. 1(c)] and two orthogonal polarization components of the speckle are found uncorrelated. At difference of recent studies of vector beams in complex media [27], our experiments refer to strong coupling (two-sided channel).

To model the scattering of mosaic vector beams, we consider the monochromatic paraxial field $\mathbf{\Psi}(\mathbf{x}, z_0)$ impinging on the diffuser at position $z = z_0$, which in quantumlike notation writes as

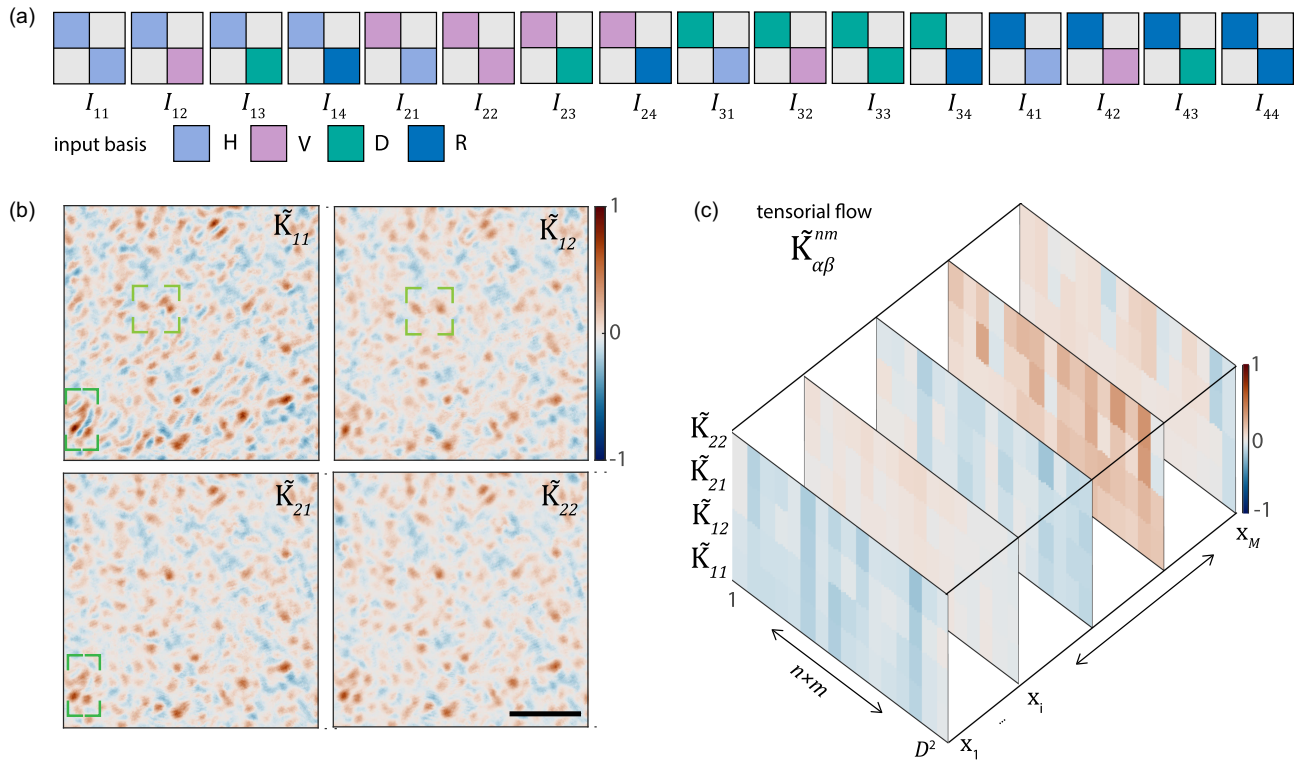

FIG. 2. Experimental measurement of the tensorial flow. (a) Scheme of the 16 input mosaic beams used to measure the transmission matrices $\tilde{K}^{14}_{\alpha\beta}$ when $D = 4$. H, V, D, and R, indicate horizontal, vertical, diagonal, and right-circular SOP. (b) Example of the four measured matrices $\tilde{K}^{14}_{\alpha\beta}$. Data are normalized to the absolute maximum. Colored boxes highlight differences between the components in the same spatial regions. Scale bar is 1 mm. (c) Graphical representation of the entire measured tensor $\tilde{K}^{nm}_{\alpha\beta}$, obtained by contracting the n and m indices and unfolding the spatial vector $\mathbf{x}$ in $M = 64\,000$ points.

$$|\Psi(z_0)\rangle = \sum_{n=1}^{D}\sum_{\alpha=1}^{2} a^n_\alpha A_n e^{i\chi_n}|\alpha\rangle|n\rangle, \tag{1}$$

where D is the number of tesserae in the mosaic, n the tessera index, α the polarization index, being $\hat{\mathbf{a}}^n = \hat{\mathbf{e}}_1 a^n_1 + \hat{\mathbf{e}}_2 a^n_2$ the polarization of the nth tessera, and $A_n = \sqrt{I_n}$ and χ_n the laser amplitude and phase over the nth spatial domain (see Supplemental Material [30]). The field in Eq. (1) exhibits nonseparable correlations between polarization and spatial modes (nonzero vectorness), which can be quantified by using quantum-inspired metrics [37–39]. The diffuser acts as a unitary operator, $\hat{D}$, and the field at a distance $z - z_0$ from the diffuser is $|\Psi(z)\rangle = \hat{U}(z - z_0)\hat{D}|\Psi(z_0)\rangle$, where $\hat{U}$ is the Fresnel propagation operator. The operator $\hat{D}$ is not separable and applies to the entire field, and thus represents a two-sided channel. By defining the effective scattering operator

$$\hat{K}(\mathbf{x}, z) = \sum_{\alpha=1}^{2} \hat{D}^\dagger \hat{U}^\dagger(z - z_0)|\alpha, \mathbf{x}\rangle\langle\alpha, \mathbf{x}|\hat{U}(z - z_0)\hat{D}, \tag{2}$$

the point-dependent transmitted intensity is

$$I(\mathbf{x}, z) = \sum_{n,m=1}^{D}\sum_{\alpha,\beta=1}^{2} \overline{c^n_\alpha}\, K^{mn}_{\alpha\beta}(\mathbf{x}, z) c^m_\beta, \tag{3}$$

$K^{nm}_{\alpha\beta}(\mathbf{x}, z) = \langle\alpha, n|\hat{K}(\mathbf{x}, z)|\beta, m\rangle$ and $c^n_\alpha = a^n_\alpha A_n e^{i\chi_n}$. We refer to $K^{nm}_{\alpha\beta}$ as the transmission tensor, being n, m the tesserae and α, β the polarization indices. $K^{nm}_{\alpha\beta}$ is composed by D^2 complex-valued matrices of size 2×2 for each spatial point $\mathbf{x}$. The tensor is Hermitian: $K^{nm}_{\alpha\beta} = \overline{K^{mn}_{\beta\alpha}}$. This operator generalizes the transmission matrix [40] and its vectorial extension [41] to input polarization modes and output intensity modes. The rank of $K^{nm}_{\alpha\beta}$ is 4 times larger than the corresponding transmission matrix for the same number of input modes. Equation (3) reveals that the pointwise intensity is a function of all the SOPs of the input mosaic. The entire polarization information is encoded in every point of any single speckle pattern. Therefore, $K^{nm}_{\alpha\beta}$ fully characterizes the disordered channel.

We develop a simple and rapid method to measure the real tensor $\Re\{K^{nm}_{\alpha\beta}\} = \tilde{K}^{nm}_{\alpha\beta}$ for arbitrary D. We call $\tilde{K}^{nm}_{\alpha\beta}$ tensorial flow. We experimentally prove that the tensorial flow is an effective quantity for controlling the transmission

of the mosaic beam and for decoding the original polarization structure. Our technique obtains $\tilde{K}^{nm}_{\alpha\beta}$ algebraically from a minimal set of intensity measurements with prepared input SOPs. The experimental procedure is explained in Supplemental Material [30]. The method is scalable: to determine the element $\tilde{K}^{nm}_{\alpha\beta}$ we need to vary only the polarization of the nth and mth tessera at constant χ_n and A_n. We prepare the n part and m part of the mosaic in the states $\hat{\mathbf{a}}^n = \hat{\mathbf{a}}_i =$ and $\hat{\mathbf{a}}^m = \hat{\mathbf{a}}_j$, where $i, j = 1, \ldots, 4$ denotes the indices of three mutually unbiased bases, e.g., horizontal (H), vertical (V), diagonal (D), and right-circular (R) polarization. The SOP of the remaining $D-2$ input parts is chosen arbitrarily and kept constant. We measure the corresponding intensity patterns I_{ij}. The tensor components of indices n and m are obtained in compact form as

$$\tilde{K} = P^T I_{\text{exp}} P, \tag{4}$$

where P is a matrix of real coefficients and I_{exp} is made by 16 intensity measurements I_{ij} $(i, j = 1, ..4)$. To give an example, Fig. 2(a) illustrates the SOPs of the 16 input mosaics used to measure the tensor component $\tilde{K}^{14}_{\alpha\beta}$ when $D = 4$. The resulting spatially resolved $\tilde{K}^{14}_{\alpha\beta}$ is shown in Fig. 2(b) by using four intensity maps. Each map gives the normalized contribution to the intensity that comes from the polarization components of that couple of tesserae. To obtain the full tensorial flow, we measure D^2 matrices as in Fig. 2(b) by varying the tessera indices and keeping fixed the polarization bases. Figure 2(c) reports a four-dimensional view of the entire $\tilde{K}^{nm}_{\alpha\beta}$ measured for $D = 4$.

We validate the measured tensor by showing that it accurately characterizes vector beam propagation through the diffuser. We generate an arbitrary mosaic beam encoding four SOPs [Fig. 3(a)] and we use the data in Fig. 2(c) to predict the intensity pattern on the output plane. We directly apply Eq. (3) by summing all the 64 terms. The result is shown in Fig. 3. We find a very good agreement between the predicted output [Fig. 3(b)] and the direct measurement [Fig. 3(c)]. The small-scale features of the speckle pattern are successfully reproduced, with the position of most speckles that coincides. Bright spots are found with high precision, while the discrepancy is visually more evident in low-intensity regions where noise has a larger effect. The correlation between the images is $\rho = 0.67$, to be compared with $\rho \simeq 0$ given by two independent speckle patterns with the same spatial coherence. The average root-mean-square error is RMSE $= 0.06$. These quantities furnish a figure of merit on the accuracy of the measured $\tilde{K}^{nm}_{\alpha\beta}$. The precision is mainly limited by the fidelity of the input mosaic beams, which is affected by the uncertainty on the generated SOPs and the inhomogeneity of the beam intensity. The result proves that $\tilde{K}^{nm}_{\alpha\beta}$ is effective in modeling the experimental

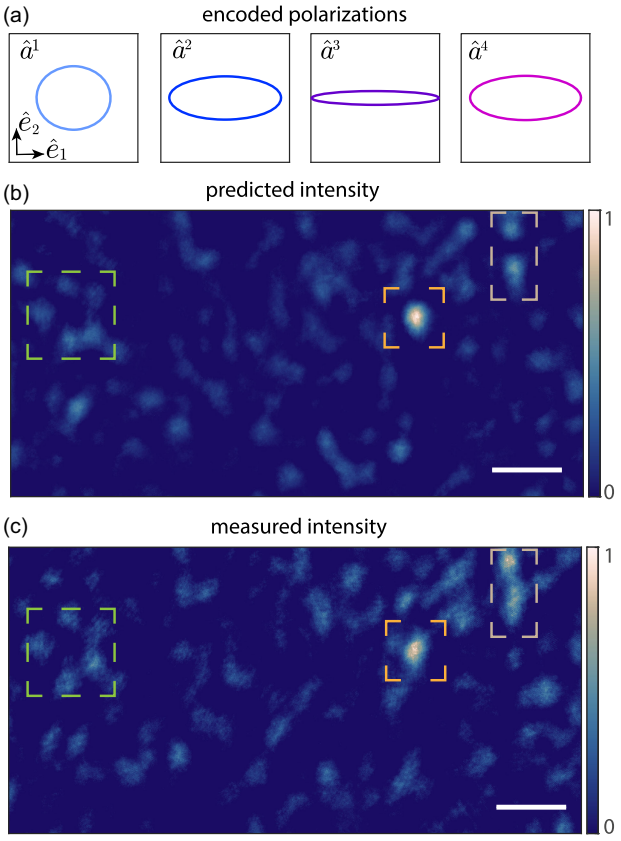

FIG. 3. Experimental validation of the measured tensorial flow. We predict the intensity scattered by a diffuser for any input SOPs. (a) Polarization ellipses showing the four SOPs encoded in a mosaic beam with $D = 4$. (b) Intensity pattern calculated from the measured tensor $\tilde{K}^{nm}_{\alpha\beta}$. (c) Measured intensity as received on the camera plane. Colored boxes highlight the same distinctive small-scale features in the predicted and measured speckle pattern. Scale bars are 200 μm.

channel and underlines the robustness of our measurement method.

We exploit the measured $\tilde{K}^{nm}_{\alpha\beta}$ to demonstrate the decoding of the input SOPs from the scattered intensity. We consider the inverse problem for Eq. (3), i.e., obtaining all the coefficients a^n_α and a^n_β by a single-shot measurement of $I(\mathbf{x})$. We solve the problem numerically by constructing a linear system with complex variables $w^{nm}_{\alpha\beta} = \overline{a^n_\alpha} a^m_\beta$ and applying the constraint $|a^n_1| + |a^n_2| = 1$ on the real and imaginary part of each $w^{nm}_{\alpha\beta}$. Figure 4 shows that we are able to retrieve the input polarization structure. The polarization message, composed of four SOPs [Fig. 4(a)], is received as a speckle intensity [Fig. 4(b)], from which we get the polarization ellipses in Fig. 4(c). This proves simultaneous and accurate transfer of multiple polarizations through strong disorders. The polarization string is decoded with an overall error $E = \sum_{n=1}^{D} \Delta S^n / D = 0.09$, being ΔS^n the Euclidean distance between the encoded and decoded nth Stokes vector. We compare the error with a supervised

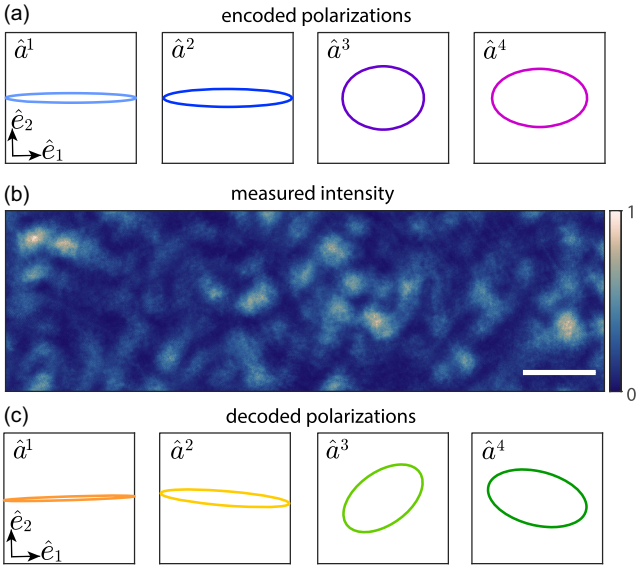

FIG. 4. Decoding vector beams in complex media. (a) Input message encoded in four SOPs ($D = 4$). (b) Intensity distribution detected after the scattering medium. (c) Polarization ellipses deciphered from the received image by using the tensorial flow $\tilde{K}^{nm}_{\alpha\beta}$. Scale bar is 200 μm.

learning reconstruction [29] that employs the same number of measurements necessary for obtaining $\tilde{K}^{nm}_{\alpha\beta}$ (256 for $D = 4$). Requiring thousands of measured data for training to operate with high precision, the performance of the neural network is poor when based only on 256 samples [29]. The transmission tensor method achieves two times larger accuracy. From the achieved decoding precision, we estimate that each polarization mode can carry nearly 7 bits of information. The capacity of the multimode link can be augmented further in a simple way by increasing D.

In conclusion, we have reported the first measurement of the tensorial flow of mosaic vector beams in a disordered medium. Our transmission tensor is a novel tool for measuring and controlling the large-scale evolution of complex data within complex media, potentially impacting schemes in cryptography [42], imaging [43] and quantum optical communication [44]. We have demonstrated that the measured tensor enables the decoding of polarization structures in strongly scattering channels. The result opens the route to polarization-based optical communication through links of practical interest.

The framework here presented applies to a wide range of disordered channels, encompassing turbulent free-space links and multimode fibers, and can be extended to nonlinear disordered media [45]. Our method, characterized by both speed and scalability, finds broad utility in photonic devices that leverage large-rank datasets. As an illustrative example, our demonstration of vector beam delivery through disorder (as depicted in Fig. 4) materializes as a practical realization of polarization-based optical encryption, with the transmission tensor serving as an enhanced security key. Moreover, within the realm of optical computing, the large rank of the transmission tensor can furnish additional functionalities in photonic Ising machines [46–49] and learning machines [50–53]. The characterization of mosaic vector beams not only advances our fundamental understanding of light in complex media but also opens a wealth of possibilities for applications across various scientific areas.

We acknowledge financial support from the European Uninon—Next Generation EU—by the Italian Ministry of University and Research (MUR) under PRIN 2022—No. 2022N738SA. Color maps are produced with Scientific colour maps [54].

*davide.pierangeli@roma1.infn.it

[1] M. R. Dennis, K. O'Holleran, and M. J. Padgett, Singular optics: Optical vortices and polarization singularities, Prog. Opt. **53**, 293 (2009).
[2] Q. Zhan, Cylindrical vector beams: From mathematical concepts to applications, Adv. Opt. Photonics **1**, 1 (2009).
[3] C. Rosales-Guzmán, B. Ndagano, and A. Forbes, A review of complex vector light fields and their applications, J. Opt. **20**, 123001 (2018).
[4] V. D'Ambrosio, N. Spagnolo, L. Del Re, S. Slussarenko, Y. Li, L. C. Kwek, L. Marrucci, S. P. Walborn, L. Aolita, and F. Sciarrino, Photonic polarization gears for ultra-sensitive angular measurements, Nat. Commun. **4**, 2432 (2013).
[5] F. Töppel, A. Aiello, C. Marquardt, E. Giacobino, and G. Leuchs, Classical entanglement in polarization metrology, New J. Phys. **16**, 073019 (2014).
[6] S. Berg-Johansen, F. Töppel, B. Stiller, P. Banzer, M. Ornigotti, E. Giacobino, G. Leuchs, A. Aiello, and C. Marquardt, Classically entangled optical beams for high-speed kinematic sensing, Optica **2**, 864 (2015).
[7] S. Sederberg, F. Kong, F. Hufnagel, C. Zhang, E. Karimi, and P. B. Corkum, Vectorized optoelectronic control and metrology in a semiconductor, Nat. Photonics **14**, 680 (2020).
[8] L. Fang, Z. Wan, A. Forbes, and J. Wang, Vectorial doppler metrology, Nat. Commun. **12**, 4186 (2021).
[9] R. Barboza, A. Babazadeh, L. Marrucci, F. Cardano, C. de Lisio, and V. D'Ambrosio, Ultra-sensitive measurement of transverse displacements with linear photonic gears, Nat. Commun. **13**, 1080 (2022).
[10] F. Castellucci, T. W. Clark, A. Selyem, J. Wang, and S. Franke-Arnold, Atomic compass: Detecting 3D magnetic field alignment with vector vortex light, Phys. Rev. Lett. **127**, 233202 (2021).
[11] V. D'Ambrosio, E. Nagali, S. P. Walborn, L. Aolita, S. Slussarenko, L. Marrucci, and Fabio Sciarrino, Complete experimental toolbox for alignment-free quantum communication, Nat. Commun. **3**, 961 (2012).
[12] V. Parigi, V. D'Ambrosio, C. Arnold, L. Marrucci, F. Sciarrino, and J. Laurat, Storage and retrieval of vector beams of light in a multiple-degree-of-freedom quantum memory, Nat. Commun. **6**, 7706 (2015).

[13] J. Liu, I. Nape, Q. Wang, A. Vallés, J. Wang, and A. Forbes, Multidimensional entanglement transport through single-mode fiber, Sci. Adv. **6**, eaay0837 (2020).
[14] J. Ishihara, T. Mori, T. Suzuki, S. Sato, K. Morita, M. Kohda, Y. Ohno, and K. Miyajima, Imprinting spatial helicity structure of vector vortex beam on spin texture in semiconductors, Phys. Rev. Lett. **130**, 126701 (2023).
[15] G. Milione, T. A. Nguyen, J. Leach, D. A. Nolan, and R. R. Alfano, Using the nonseparability of vector beams to encode information for optical communication, Opt. Lett. **40**, 4887 (2015).
[16] Y. Zhao and J. Wang, High-base vector beam encoding/decoding for visible-light communications, Opt. Lett. **40**, 4843 (2015).
[17] G. Milione *et al.*, 4×20 Gbit/s mode division multiplexing over free space using vector modes and a q-plate mode (de) multiplexer, Opt. Lett. **40**, 1980 (2015).
[18] J. Liu *et al.*, Direct fiber vector eigenmode multiplexing transmission seeded by integrated optical vortex emitters, Light **7**, 17148 (2018).
[19] Z. Zhu, M. Janasik, A. Fyffe, D. Hay, Y. Zhou, B. Kantor, T. Winder, R. W. Boyd, G. Leuchs, and Z. Shi, Compensation-free high-dimensional free-space optical communication using turbulence-resilient vector beams, Nat. Commun. **12**, 1666 (2021).
[20] B. Ndagano, B. Perez-Garcia, F. S. Roux, M. McLaren, C. Rosales-Guzman, Y. Zhang, O. Mouane, R. I. Hernandez-Aranda, T. Konrad, and A. Forbes, Characterizing quantum channels with non-separable states of classical light, Nat. Phys. **13**, 397 (2017).
[21] A. Sit *et al.*, High-dimensional intracity quantum cryptography with structured photons, Optica **4**, 1006 (2017).
[22] J. Li, Y. C. Hung, O. Kulce, D. Mengu, and A. Ozcan, Polarization multiplexed diffractive computing: All-optical implementation of a group of linear transformations through a polarization-encoded diffractive network, Light Sci. Appl. **11**, 153 (2022).
[23] Y. Li, J. Li, Y. Zhao, T. Gan, J. Hu, M. Jarrahi, and A. Ozcan, Universal polarization transformations: Spatial programming of polarization scattering matrices using a deep learning-designed diffractive polarization transformer, Adv. Mater. **35**, 2303395 (2023).
[24] I. Gianani *et al.*, Transmission of vector vortex beams in dispersive media, Adv. Opt. Photonics **2**, 036003 (2020).
[25] F. Hufnagel, A. Sit, F. Bouchard, Y. Zhang, D. England, K. Heshami, B. J. Sussman, and E. Karimi, Investigation of underwater quantum channels in a 30 meter flume tank using structured photons, New J. Phys. **22**, 093074 (2020).
[26] C. Peters, M. Cox, A. Drozdov, and A. Forbes, The invariance and distortion of vectorial light across a real-world free space link, Appl. Phys. Lett. **123**, 021103 (2023).
[27] I. Nape *et al.*, Revealing the invariance of vectorial structured light in complex media, Nat. Photonics **16**, 538 (2022).
[28] K. Singh, I. Nape, W. T. Buono, A. Dudley, and A. Forbes, A robust basis for multi-bit optical communication with vectorial light, Laser Photonics Rev. **17**, 2200844 (2023).
[29] D. Pierangeli and C. Conti, Single-shot polarimetry of vector beams by supervised learning, Nat. Commun. **14**, 1831 (2023).
[30] See Supplemental Material at http://link.aps.org/supplemental/10.1103/PhysRevLett.132.243801 for details on the experimental setup, the scattering theory of mosaic vector beams, the method for measuring the transmission tensor and decoding the polarizations, which includes Refs. [31–33].
[31] I. Freund, Stokes-vector reconstruction, Opt. Lett. **15**, 1425 (1990).
[32] T. Kohlgraf-Owens and A. Dogariu, Spatially resolved scattering polarimeter, Opt. Lett. **34**, 1321 (2009).
[33] M. Facchin, G. D. Bruce, and K. Dholakia, Speckle-based determination of the polarisation state of single and multiple laser beams, OSA Continuum **3**, 1302 (2020).
[34] R. M. A. Azzam, Stokes-vector and Mueller-matrix polarimetry, J. Opt. Soc. Am. A **33**, 1396 (2016).
[35] B. Schaefer, E. Collett, R. Smyth, D.Barrett, and B. Frahar, Measuring the Stokes polarization parameters, Am. J. Phys. **75**, 2 (2007).
[36] H. B. de Aguiar, S. Gigan, and S. Brasselet, Polarization recovery through scattering media, Sci. Adv. **3**, e1600743 (2017).
[37] A. Aiello, F. Töppel, C. Marquardt, E. Giacobino, and G. Leuchs, Quantum-like nonseparable structures in optical beams, New J. Phys. **17**, 043024 (2015).
[38] A. Selyem, C. Rosales-Guzmán, S. Croke, A. Forbes, and S. Franke-Arnold, Basis-independent tomography and non-separability witnesses of pure complex vectorial light fields by Stokes projections, Phys. Rev. A **100**, 063842 (2019).
[39] A. Aiello, X. B. Hu, V. Rodríguez-Fajardo, A. Forbes, R. I. Hernandez-Aranda, B. Perez-Garcia, and C. Rosales-Guzmán, A non-separability measure for spatially disjoint vectorial fields, New J. Phys. **24**, 063032 (2022).
[40] S. M. Popoff, G. Lerosey, R. Carminati, M. Fink, A. C. Boccara, and S. Gigan, Measuring the transmission matrix in optics: An approach to the study and control of light propagation in disordered media, Phys. Rev. Lett. **104**, 100601 (2010).
[41] S. Tripathi, R. Paxman, T. Bifano, and K. C. Toussaint, Vector transmission matrix for the polarization behavior of light propagation in highly scattering media, Opt. Express **20**, 16067 (2012).
[42] A. Di Falco, V. Mazzone, A. Cruz, and A. Fratalocchi, Perfect secrecy cryptography via mixing of chaotic waves in irreversible time-varying silicon chips, Nat. Commun. **10**, 5827 (2019).
[43] S. Gigan *et al.*, Roadmap on wavefront shaping and deep imaging in complex media, J. Phys. Photonics **4**, 042501 (2022).
[44] N. Herrera Valencia, S. Goel, W. McCutcheon, H. Defienne, and M. Malik, Unscrambling entanglement through a complex medium, Nat. Phys. **16**, 1112 (2020).
[45] J. Moon, Y.-C. Cho, S. Kang, M. Jang, and W. Choi, Measuring the scattering tensor of a disordered nonlinear medium, Nat. Phys. **19**, 1709 (2023).
[46] D. Pierangeli, G. Marcucci, and C. Conti, Large-scale photonic ising machine by spatial light modulation, Phys. Rev. Lett. **122**, 213902 (2019).
[47] D. Pierangeli, M. Rafayelyan, C. Conti, and S. Gigan, Scalable spin-glass optical simulator, Phys. Rev. Appl. **15**, 034087 (2021).

[48] Y. Fang, J. Huang, and Z. Ruan, Experimental observation of phase transitions in spatial photonic ising machine, Phys. Rev. Lett. **127**, 043902 (2021).

[49] H. Yamashita, K. I. Okubo, S. Shimomura, Y. Ogura, J. Tanida, and H. Suzuki, Low-rank combinatorial optimization and statistical learning by spatial photonic Ising machine, Phys. Rev. Lett. **131**, 063801 (2023).

[50] G. Marcucci, D. Pierangeli, and C. Conti, Theory of neuromorphic computing by waves: Machine learning by rogue waves, dispersive shocks, and solitons, Phys. Rev. Lett. **125**, 093901 (2020).

[51] U. Tegin, M. Yildirim, I. Oguz, C. Moser, and D. Psaltis, Scalable optical learning operator, Nat. Computat. Sci. **1**, 542 (2021).

[52] M. Rafayelyan, J. Dong, Y. Tan, F. Krzakala, and S. Gigan, Large-scale optical reservoir computing for spatiotemporal chaotic systems prediction, Phys. Rev. X **10**, 041037 (2020).

[53] D. Pierangeli, G. Marcucci, and C. Conti, Photonic extreme learning machine by free-space optical propagation, Photonics Res. **9**, 1446 (2021).

[54] F. Crameri, Scientific colour maps, Zenodo, 10.5281/zenodo.1243862 (2018).